nature communications

Article

https://doi.org/10.1038/s41467-024-53561-2

A splicing isoform of PD-1 promotes tumor progression as a potential immune checkpoint

Received: 22 November 2023

Accepted: 16 October 2024

Published online: 23 October 2024

Check for updates

Xuetong Wang[1,2,3], Tongfeng Liu[3,4], Yifei Li[3,5], Ao Ding[3,5], Chang Zhang[3,6], Yinmin Gu[3], Xujie Zhao[3], Shuwen Cheng[3,7], Tianyou Cheng[8], Songzhe Wu[3], Liqiang Duan[8], Jihang Zhang[3,4], Rong Yin[9], Man Shang[10] & Shan Gao[1,2,3]

The immune checkpoint receptor, programmed cell death 1 (PD-1, encoded by *PDCD1*), mediates the immune escape of cancer, but whether PD-1 splicing isoforms contribute to this process is still unclear. Here, we identify an alternative splicing isoform of human PD-1, which carries a 28-base pairs extension retained from 5′ region of intron 2 (PD-1^28), is expressed in peripheral T cells and tumor infiltrating lymphocytes. PD-1^28 expression is induced on T cells upon activation and is regulated by an RNA binding protein, TAF15. Functionally, PD-1^28 inhibits T cell proliferation, cytokine production, and tumor cell killing in vitro. In vivo, T cell-specific exogenous expression of PD-1^28 promotes tumor growth in both a syngeneic mouse tumor model and humanized NOG mice inoculated with human lung cancer cells. Our study thus demonstrates that PD-1^28 functions as an immune checkpoint, and may contribute to resistance to immune checkpoint blockade therapy.

T cell activation is mediated by T cell receptor (TCR), co-stimulatory molecules, and immune checkpoint (IC) molecules to maintain immune homeostasis[1,2]. The programmed cell death-1 (PD-1) receptor is one of the IC molecules and expressed by activated T cells, B cells, natural killer T cells, and cancer cells, etc.[3–5]. PD-1 negatively regulates the function of T cells via engaging its two ligands, PD-1 ligand 1 (PD-L1) or PD-L2, which is expressed by cancer cells to evade immune elimination[6,7]. A low response rate or even resistance to IC inhibitors (ICI) targeting the PD-1/PD-L1 indicates the urgent need to identify new IC genes and dissect their potential mechanisms[8,9].

Alternative splicing (AS) is a process in which the same precursor-mRNAs (pre-mRNA) can be spliced into different combinations to produce mRNA and protein isoforms with different functions and subcellular localization[10,11]. AS is involved in regulating the function of physiology or pathology, including cancer[12,13] and also plays an important role in the expression of IC molecules[14,15]. Previous studies revealed that *PDCD1* has several isoforms by jumping distinct exons[16–18], however, whether there are more new isoforms is needed to be explored. The potential molecular functions of these isoforms have completely unknown.

In this study, we identify a novel PD-1 isoform, which negatively regulates T cell function and promotes tumor progression as a potential immune checkpoint. Our study sheds light on our understanding of T cell regulation and may provide a new target for IC therapy.

[1]School of Biomedical Engineering (Suzhou), Division of Life Sciences and Medicine, University of Science and Technology of China, Hefei, China. [2]Suzhou Institute of Biomedical Engineering and Technology, Chinese Academy of Science, Suzhou, China. [3]Zhongda Hospital, School of Life Sciences and Technology, Advanced Institute for Life and Health, Southeast University, Nanjing, China. [4]Medical School of Guizhou University, Guiyang, China. [5]School of Pharmacy, Nanjing University of Chinese Medicine, Nanjing, China. [6]Department of medical oncology, The Key Laboratory of Advanced Interdisciplinary Studies Center, State Key Laboratory of Respiratory Disease, The First Affiliated Hospital of Guangzhou Medical University, Guangzhou Medical University, Guangdong, China. [7]Medical School of Nanjing University, Nanjing, China. [8]Shanxi Academy of Advanced Research and Innovation, Taiyuan, China. [9]Nanjing Medical University Affiliated Cancer Hospital, Nanjing, China. [10]Nanjing Women and Children's Healthcare Institute, Women' s Hospital of Nanjing Medical University (Nanjing Women and Children' s Healthcare Hospital), Nanjing, China. e-mail: gaos@sibet.ac.cn

Results

The identification of a novel PD-1 isoform

In an effort to amplify *PDCD1* from peripheral blood mononuclear cells (PBMC) of a healthy human donor, we unexpectedly found a novel splicing isoform using reverse transcription-PCR (RT-PCR) with Sanger sequencing (Supplementary Fig. 1A-C), which showed that this novel isoform retained 28 base pairs (bp) from the start of the *PDCD1* intron 2 (Fig. 1A). This new isoform contains signal peptide, immunoglobulin variable (IgV) domain and a new cytoplasmic tail with different amino acid sequence from PD-1 (252 amino acids) (Fig. 1B, Supplementary Fig. 1D, and Supplementary Table S1). Therefore, we named this PD-1 isoform as PD-1^28. To further confirm this, RT-PCR coupled with Sanger sequencing verified the expression of *PDCD1^28* in a variety of human leukemia cell lines (Supplementary Fig. 1E). We further performed 5′- and 3′-rapid amplification of cDNA ends (RACE) and found that *PDCD1^28* was a 2,124-nt transcript with five exons (Supplementary Fig. 1F, G and Supplementary Table S2). Together, our results identify a new splicing isoform of *PDCD1*, named as *PDCD1^28*.

For specific recognition of the endogenous authentic PD-1^28, we used the distinct 107 amino acid fragment from PD-1^28 cytoplasmic tail, a part of 252 amino acids, as an antigen to generate custom antibodies. We obtained monoclonal and polyclonal antibodies and verified that PD-1^28 could be specifically recognized through immunoprecipitation followed by immunoblot (Supplementary Fig. 1H, I). One of the monoclonal antibodies was used in flow cytometry (FACS) (Supplementary Fig. 1J). In addition, we established two *PDCD1* knockout (KO) Jurkat cell lines, KO-1 and KO-2, as the negative control, using CRISPR-Cas9 system (Supplementary Fig. 1K, L). To further verify the endogenous presence of PD-1^28, we performed an immunoprecipitation followed by immunoblot and mass spectrometry (Fig. 1C, D), which detected specific peptides for PD-1^28 cytoplasmic tail (Fig. 1E). Immunofluorescence revealed that PD-1^28 was mainly located in the cytoplasm of Jurkat cells stimulated with PHA, whereas we could hardly detect it in unstimulated condition (Fig. 1F). We simultaneously detected the localization of PD-1 and PD-1^28 in Jurkat cells activated by PHA, suggesting that they have different cellular localization (Supplementary Fig. 1M). We then hypothesized that PD-1^28 might be induced upon T cell activation in a similar way as PD-1[3,19]. In this regard, we activated T cells using three classic methods: CD3 and CD28, PMA and ionomycin, and PHA. Both mRNA and protein levels of the PD-1^28 were elevated after Jurkat cell activation (Fig. 1G–L), and we also observed an increase in the copy numbers of *PDCD1^28* upon CD3 and CD28 stimulation (Supplementary Fig. 1O). To explore whether the intron retention is more prominently activated, we compared the percent splice in (PSI) values of *PDCD1^28* and *PDCD1*, suggesting intron retention is less pronounced (Supplementary Fig. 1P–R). We also performed a concurrent assessment of PD-1 and PD-1^28 in activated Jurkat cells (Fig. 1H, J, L) and human leukemia cell lines (Supplementary Fig. 1S), which showed that the protein expression level of PD-1 was higher. To evaluate the prevalence of *PDCD1^28* and other variants as well as *PDCD1*, we determined the copy numbers of *PDCD1*, *PDCD1^28*, and other variants of *PDCD1* in $CD3^+$ T cells derived from PBMCs of three healthy individuals[16] (Supplementary Fig. 1T and Supplementary Table S3), and further measured the expression of PD-1 and PD-1^28 in different populations of primary T cells with FACS (Fig. 1M), which revealed that PD-1 was relatively highly expressed compared to PD-1^28. Furthermore, we explored whether PD-1^28 is expressed in tumor-infiltrating lymphocytes (TIL) of cancer patients. FACS revealed the expression of PD-1^28 in $CD4^+$ and $CD8^+$ T cell subsets from TILs derived from seven lung cancer samples (Fig. 1N and Supplementary Table S4). Overall, these data demonstrate that PD-1^28 is a novel isoform of PD-1 and is expressed in subpopulations of T lymphocytes.

Splicing of PDCD1^28 is regulated by TAF15

To identify the splicing factors responsible for generating *PDCD1^28*, we selected a region covering the upstream and downstream 200 bp of *PDCD1^28* specific 28 bp (428 bp in total) to predict potential RNA binding proteins (RBP) using RBPsuite, RBPmap and StarBase database, which revealed three putative RBPs, FUS, EWSR1, and TAF15 as potential splicing factors (Fig. 2A). To experimentally verify this, we used two distinct short hairpin RNAs (shRNA) to knock down endogenous *FUS*, *EWSR1*, and *TAF15* in Jurkat cells (Fig. 2B and Supplementary Fig. 2A, B) and found that only knockdown (KD) of *TAF15*, but not the other two candidates reduced the concomitant mRNA and protein levels of PD-1^28 (Fig. 2C–H). Thus, we focused on TAF15 for the following study. In contrast, overexpression (OE) of *TAF15* increased both mRNA and protein levels of PD-1^28 (Fig. 2I–K). To evaluate whether *TAF15* affects the splicing activity of *PDCD1^28*, we measured the PSI values for *PDCD1^28* splicing event in *TAF15* KD or OE cells and observed that *TAF15* KD reduced the PSI of *PDCD1^28*, while *TAF15* OE increased PSI (Supplementary Fig. 2C, D). To further elucidate the activation mechanism of *PDCD1^28* with *TAF15*, we knocked down and overexpressed *TAF15* in Jurkat cells and found that the changes of *TAF15* did not affect the mRNA or protein expression levels of PD-1 (Supplementary Fig. 2E–H). Furthermore, RNA immunoprecipitation (RIP) assay demonstrated a significantly higher enrichment of TAF15 binding at endogenous *PDCD1^28* pre-mRNA compared to control (Fig. 2L). Next, we generated a *minigene* reporter containing exons 1–5 and intron 2 of *PDCD1*. We stably overexpressed the *minigene* in HEK293T cells and found that *PDCD1^28* pre-mRNA was preferentially bound by TAF15 in comparison with IgG control (Fig. 2M). On the basis of this *minigene* reporter system, *TAF15* KD led to reduced splicing of *PDCD1^28* (Fig. 2N and Supplementary Fig. 2I–K), while OE of *TAF15* resulted in increased retention of distinct 28 bp (Fig. 2O and Supplementary Fig. 2M–O). However, the changes in *TAF15* did not affect the expression of *PDCD1* (Supplementary Fig. 2L, P). Altogether, these data suggest that the splicing of *PDCD1^28* is regulated by the RBP TAF15.

PD-1^28 negatively regulates the immune function of T cells

To explore the potential underlying function of PD-1^28 in T cells, we applied two shRNAs targeting the different sequences of *PDCD1^28* unique 28 bp to knock down endogenous *PDCD1^28* in Jurkat cells. The mRNA and protein levels of PD-1^28 were correspondingly reduced in PD-1^28-KD cells compared to control cells (Fig. 3A, B), without influencing PD-1 protein level (Fig. 3B). *PDCD1^28* KD enhanced cell proliferation and IL-2 production in Jurkat cells (Fig. 3C, D). As expected, *PDCD1^28* KD exhibited enhanced killing ability against NCI-H1299 tumor cells (Fig. 3E). Conversely, we overexpressed *PDCD1* and *PDCD1^28* in KO-1 and KO-2 cells, respectively (Fig. 3F, G). Given its well-recognized inhibitory role in immune responses[6], *PDCD1* OE cells served as a positive control. *PDCD1^28* OE cells showed attenuated cell proliferation and cytokine production and were less effective on killing NCI-H1299 tumor cells compared to control (Fig. 3H–J). Considering that the Jurkat T cell line derived from T cell leukemia, we conducted the same functional experiments in primary T cells derived from PBMCs to explore the true function of PD-1^28. As expected, we observed the similar immune function changes in primary T cells as Jurkat cells (Fig. 4A–L). To further gain insights into the downstream signaling pathway, we performed RNA-sequencing (RNA-seq) in *PDCD1^28* OE cells. Gene expression profiling showed 1886 downregulated genes and 2249 upregulated genes (Supplementary Fig. 3A). Furthermore, Gene ontology (GO) analysis revealed an enrichment of the downregulated genes in signaling pathways associated with positive immune response, such as “adaptive immune response” and “T cell activation” (Supplementary Fig. 3B), while Gene Set Enrichment Analysis (GSEA) indicated the negative immune response in *PDCD1^28* OE cells compared to control cells (Supplementary Fig. 3C). To further elucidate how PD-1^28 exerts its immunosuppressive function in

https://doi.org/10.1038/s41467-024-53561-2

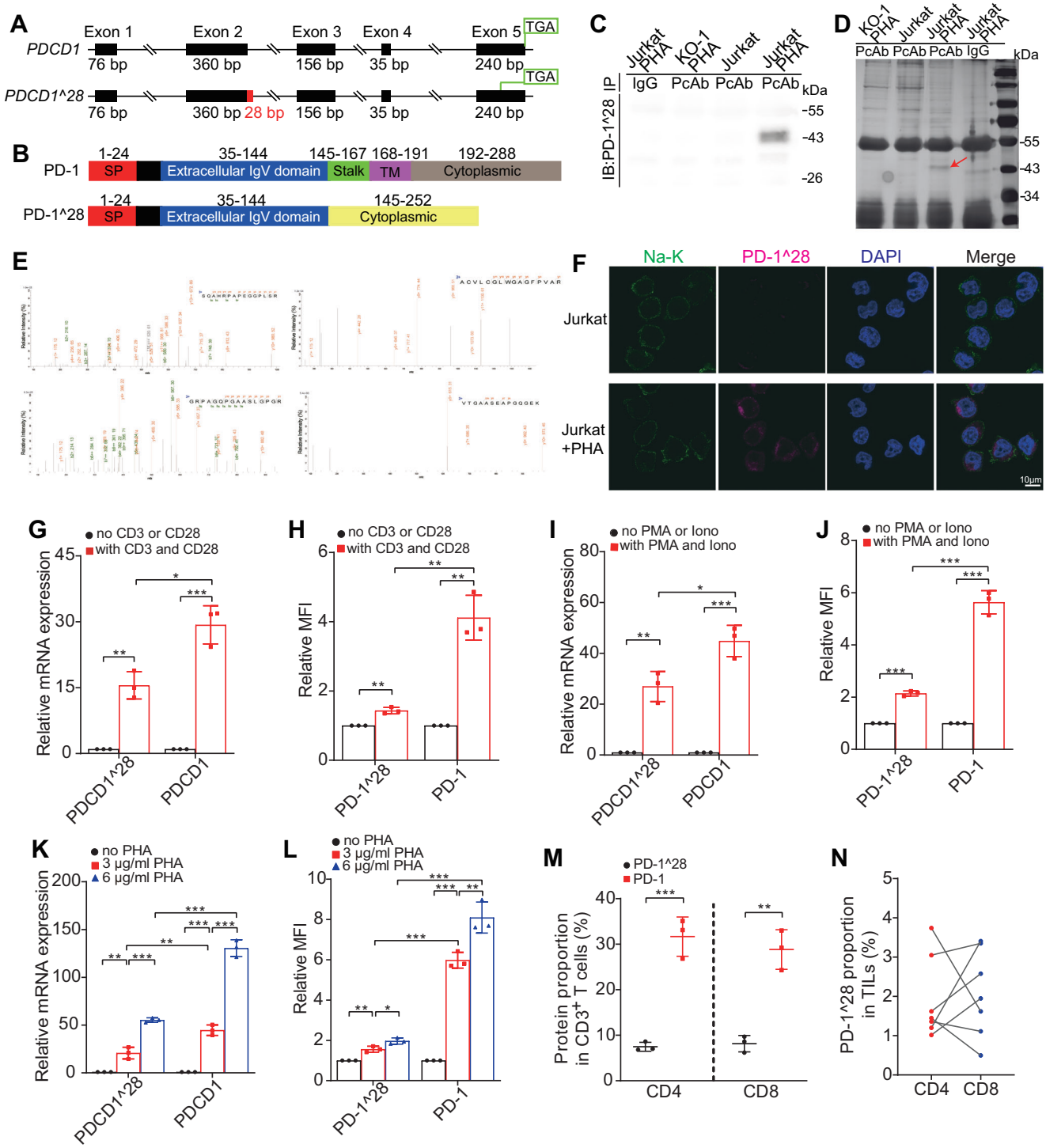

Fig. 1 | Identification and characterization of PD-1^28 in T lymphocytes. A, **B** The schematic gene structures of *PDCD1* (top) and *PDCD1^28* (bottom) (**A**) or functional domains of PD-1 (top) and PD-1^28 (bottom) (**B**). **C**, **D** Immunoblot analysis (**C**) or silver staining (**D**) of endogenous immunoprecipitation of PD-1^28 in Jurkat cells treated with PHA or vehicle for 72 h. Polyclonal antibodies (PcAb). The specific band indicated by red arrow is the PD-1^28. **E** LC-MS analysis of specific peptides for PD-1^28 cytoplasmic tail obtained from D. **F** Representative confocal images of endogenous PD-1^28 (magenta) in Jurkat cells after treatment with PHA or vehicle. The cell membranes were stained with Na/K ATPase (green). The nuclei (blue) were stained with 4′,6-diamidino-2-phenylindole (DAPI). Scale bars, 10 μm. **G**–**L** qRT-PCR analysis of *PDCD1^28* (**G**, **I**, and **K**, left) and *PDCD1* (**G**, **I**, and **K**, right) or FACS analysis of PD-1^28 (**H**, **J** and **L**, left) and PD-1 (**H**, **J** and **L**, right) and quantified as the MFI in Jurkat cells stimulated by CD3 and CD28 for 72 h (**G**, **H**), PMA and Ionomycin for 5 h (**I** and **J**) or PHA for 72 h (**K**, **L**) ($n = 3$ biologically independent experiments). **M** Quantified results of PD-1 and PD-1^28 populations in $CD4^+$ and $CD8^+$ T cells from PBMCs of 3 healthy human donors. **N** Quantified results of PD-1^28 proportion in $CD4^+$ and $CD8^+$ TILs derived from 7 lung cancer clinical specimens. Data represent the mean ± SD. Statistical significance was determined by two-tailed unpaired Student's *t*-test (**G**–**J**, **M**) or one-way ANOVA with Tukey post hoc test (**K**, **L**). $^*p < 0.05$, $^{**}p < 0.01$, $^{***}p < 0.001$. Source data, including exact *p*-values, are provided as a Source Data file.

https://doi.org/10.1038/s41467-024-53561-2

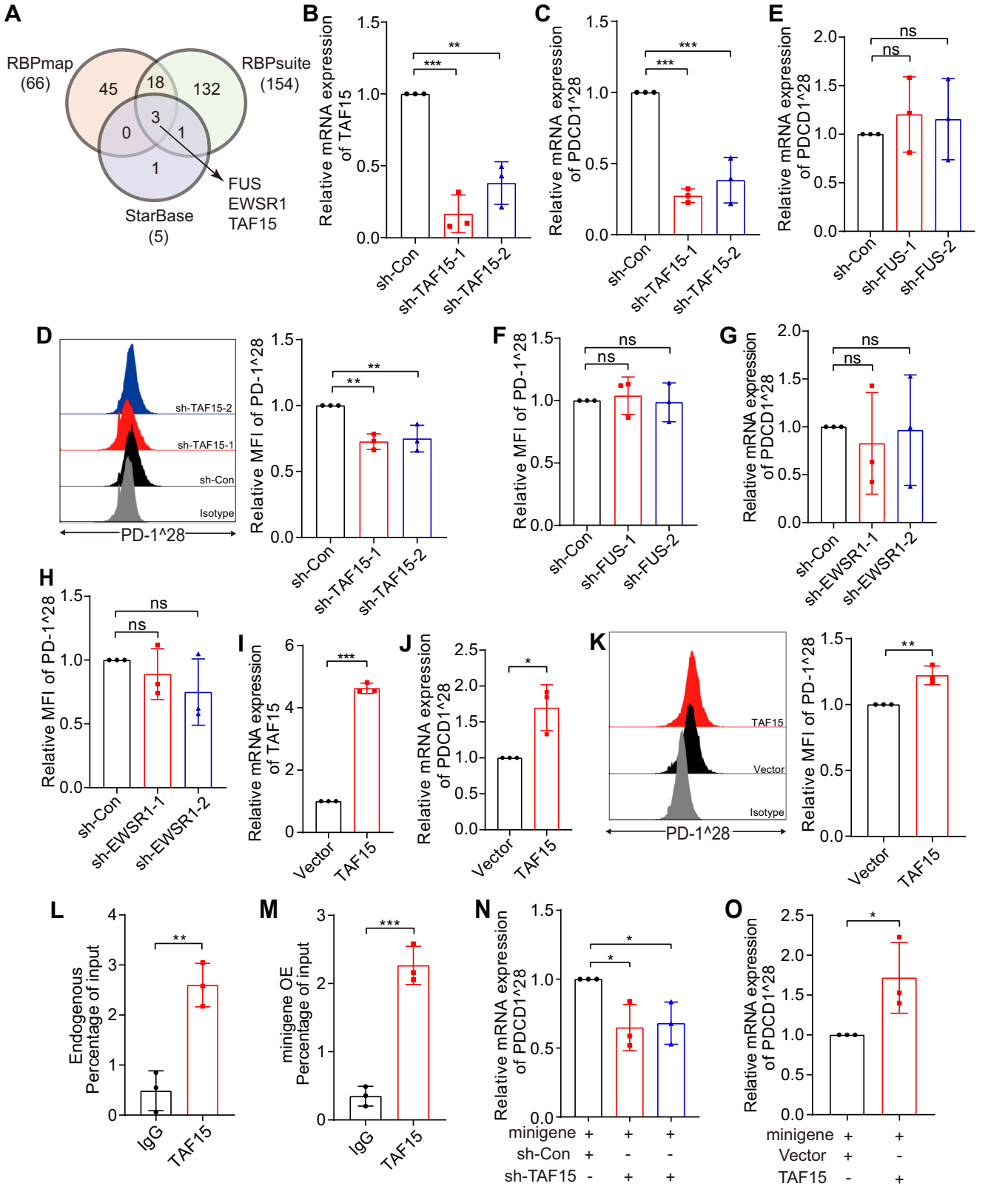

T cells, we evaluated truncated extracellular domain and cytoplasmic tail of *PDCD1^28* separately (Supplementary Fig. 4A, B). *PDCD1^28* OE cells showed attenuated cell proliferation and IL-2 production, but there were no immune function changes in extracellular or cytoplasmic tail OE cells (Supplementary Fig. 4C, D). Collectively, these results demonstrate PD-1^28 as a potential novel effector that negatively regulates the immune response of T cells.

CD28 is a well-known co-stimulatory molecule in T cell activation, while PD-1 dampens immune response as a negative regulator[20]. To further confirm the function of PD-1^28, we created two chimeric receptors consisting of the human *CD28* extracellular domain and *PDCD1^28* cytoplasmic tail (*CD28-PDCD1^28*), human *PDCD1* extracellular domain and *PDCD1^28* cytoplasmic tail (*PDCD1-PDCD1^28*). We overexpressed *CD28* as a positive control, *CD28-PDCD1^28*, *PDCD1* as a

Fig. 2 | Splicing of *PDCD1^28* is regulated by TAF15. A Venn diagram showing the three candidate RBPs. **B** qRT-PCR analysis for KD efficiency of *TAF15* in Jurkat cells transfected with the indicated shRNAs. sh-Con as a negative control ($n = 3$ biologically independent experiments). **C**, **D** qRT-PCR analysis of *PDCD1^28* (**C**) or representative FACS showing changes (**D**, left) and quantified as the MFI (**D**, right) of the PD-1^28 levels in *TAF15* KD Jurkat cells ($n = 3$ biologically independent experiments). **E**–**H** qRT-PCR analysis of *PDCD1^28* (**E**, **G**) or quantitation of PD-1^28 levels as MFI (**F**, **H**) in *FUS* (**E**, **F**) or *EWSR1* (**G**, **H**) KD Jurkat cells ($n = 3$ biologically independent experiments). **I**–**K** qRT-PCR analysis for expression levels of *TAF15* (**I**), *PDCD1^28* (**J**), or representative FACS showing changes (**K**, left) and quantified as MFI of PD-1^28 (**K**, right) in Jurkat cells transfected with the indicated plasmids ($n = 3$ biologically independent experiments). **L**, **M** RIP qRT-PCR showing the enriched binding of TAF15 on the endogenous *PDCD1^28* pre-mRNAs in Jurkat cells (**L**) or in *minigene* OE HEK293T cells (**M**) ($n = 3$ biologically independent experiments). **N**, **O** qRT-PCR analysis of *PDCD1^28* in *minigene* OE HEK293T cells with *TAF15* KD (**N**) or OE (**O**) ($n = 3$ biologically independent experiments). Data represent the mean ± SD. Statistical significance was determined by one-way ANOVA with Dunnett post hoc test (**B**–**H** and **N**) or two-tailed unpaired Student's *t*-test (**I**–**M** and **O**). $^*p < 0.05$, $^{**}p < 0.01$, $^{***}p < 0.001$. Source data, including exact *p*-values, are provided as a Source Data file.

negative control and *PDCD1-PDCD1^28* in KO-1 cells, respectively (Fig. 3K, L, O). *CD28-PDCD1^28* and *PDCD1-PDCD1^28* OE compromised cell proliferation and IL-2 production compared to control cells, while correspondingly *CD28* positively and *PDCD1* negatively regulates these processes (Fig. 3M, N, P, Q). We further fused the *PDCD1* cytoplasmic tail with the *CD28* extracellular domain (*CD28-PDCD1*), and respectively overexpressed *CD28-PDCD1* and *CD28-PDCD1^28* (Supplementary Fig. 4E), which showed that both *CD28-PDCD1* and *CD28-PDCD1^28* inhibited cell proliferation and IL-2 production compared to the control cells (Supplementary Fig. 4F and G). We next wondered whether the regulation of the alternative splicing for *PDCD1^28* is related to the immune function and performed rescue experiments. Strikingly, *PDCD1^28* OE rescued the increase of cell proliferation and IL-2 production of the *TAF15* KD (Supplementary Fig. 5A-E). Overall, these data demonstrate that PD-1^28 is a negative regulator of T cell activation.

PD-1^28 inhibits T cells activation via PD-L1

PD-L1 is a predominant ligand that engages PD-1 to exert immunosuppressive function[6,21]. It has been reported that PD-L1 exists not only on the cell membrane but also in the cytoplasm[22,23], and the IgV domain responsible for PD-1 binding to PD-L1 is retained in PD-1^28 (Fig. 1B). Therefore, we hypothesized that PD-1^28 could engage with cytoplasmic PD-L1 to exert function. To verify this hypothesis, we first performed FACS, and the data showed that the expression of PD-L1 was significantly higher in the permeabilized cells than the intact membrane cells, indicating PD-L1 is expressed in cytoplasm (Fig. 5A). We overexpressed *PDCD1^28* as well as *PDCD1* as a positive control in both KO-1 and KO-2 cells, followed by treatment with a recombinant PD-L1 Fc-fusion protein (PD-L1 immunoglobulin [Ig]) to elicit PD-1 signaling in T cells[24]. Exogenous addition of PD-L1 could not further inhibit IL-2 production in *PDCD1^28* OE cells (Fig. 5B). We first overexpressed *PDCD1^28* as well as *PDCD1* as a positive control in both KO-1 and KO-2 cells. Next, we examined the effects of simultaneous OE of *PDCD1^28* and *PDCD1LG1* (Fig. 5C, D), which suppressed cell proliferation and IL-2 production compared to single OE of either *PDCD1* or *PDCD1^28* (Fig. 5E, F).

To further understand how the binding of PD-1^28 to PD-L1 affects T cell activation, we focus on three amino acids (K78, I126, E136) of PD-1 that are critical for its binding to PD-L1 and retained in PD-1^28[25,26]. These three amino acids were then mutated into alanine (K78A, I126A, E136A) in PD-1 and PD-1^28. We stably overexpressed *PDCD1LG1* in KO-1 cells and then introduced wild-type *PDCD1^28* and mutant *PDCD1^28* as well as wild-type *PDCD1* and mutant *PDCD1* as positive controls (Fig. 5G, H). As expected, OE of wild-type *PDCD1* but not mutant *PDCD1* attenuated cell proliferation and decreased IL-2 production. In well consistence with this, OE of wild-type *PDCD1^28* but not mutant *PDCD1^28* attenuated cell proliferation and reduced IL-2 production (Fig. 5I, J). Collectively, these data suggest that the PD-1^28 and PD-L1 axis coordinate to regulate activation of T cells.

PD-1^28 effectively promotes tumor growth by reducing function of intratumoral CD8$^+$ T cells

To study the physiological function of PD-1^28, we did not find an equivalent isoform similar to *PDCD1^28* in murine *Pdcd1*. However, it has been well verified that the amino acid sequence between human PD-L1 and murine Pd-l1 is very conserved, and their overall structure is almost identical[27]. Murine Pd-l1 and human PD-L1 have the same affinity when binding to human PD-1, and murine Pd-l1/human PD-1 axis can inhibit the activation of Jurkat cells[27]. We speculated that PD-1^28 could bind to murine Pd-l1 to exert immune function. Therefore, we specifically expressed human *PDCD1^28* in mouse T cells through *PDCD1^28$^{flox/flox}$* mice crossed with *Cd4^{cre}* mice (*PDCD1^28* conditional knockin (*PDCD1^28^{CKI}*) mice) (Supplementary Fig. 6A, B). Immunoblot and FACS showed that PD-1^28-knockin did not alter the expression of Pd-1 in *PDCD1^28^{CKI}* mice (Supplementary Fig. 6B, C). Neither the development and peripheral homeostasis of T cells, nor the population of memory T cells were affected (Supplementary Fig. 6D–K). Upon stimulation with anti-CD3 and anti-CD28 antibodies, levels of proliferation and production of cytokines of naive *PDCD1^28^{CKI}* T cells were barely influenced compared to control (Supplementary Fig. 6L–O). These data show that activation of PD-1^28-knockin T cells is unaltered when the PD-1^28 pathway was not engaged.

To test the importance of PD-1^28 in anti-tumor immunity, we challenged control and *PDCD1^28^{CKI}* mice with mouse MC38 colorectal carcinoma and B16F10 melanoma models. Compared to control, *PDCD1^28^{CKI}* mice showed faster tumor progression indicated by increased tumor volume, subsequently resulting in reduced survival (Fig. 6A and Supplementary Fig. 7A–C). TILs play an essential role in anti-tumor immunity, so we explored the immune landscape of T cells in the tumor microenvironment (TME). We didn't observe notable changes either in the total numbers of tumor-infiltrating CD4$^+$ T cells and CD8$^+$ T cells or in the percentage of T_{reg} cells or in cellular proliferation of CD8$^+$ TILs (Fig. 6B–E and Supplementary Fig. 7D–F). However, frequency of TIL CD8$^+$ T cells positive for the cytolytic molecule GzmB was reduced compared to control mice (Fig. 6F), suggesting decreased cytotoxic ability. In consistence, the inflammatory cytokines interferon gamma (IFN-γ) and tumor necrosis factor (TNF) were also reduced (Fig. 6G, H). Furthermore, *PDCD1^28^{CKI}* mice showed resistance to anti-Pd-l1 therapy and dampened function of intertumoral CD8$^+$ T cells compared to control mice (Fig. 6I–L and Supplementary Fig. 7G). The population of T_{reg} cells decreased in both wild-type and *PDCD1^28^{CKI}* mice (Fig. 6M), consistent with a previous report in which checkpoint blockade therapy was used[28]. Collectively, these data demonstrate that human PD-1^28 negatively regulates T cell activation of mice.

To further confirm the intrinsic role of PD-1^28 in the anti-tumor immunity, we examined the tumorigenesis of NCI-H1299 cells in humanized PBMC (huPBMC)-NOG (NOD.Cg-PrkdcsidIL2rgtm1Sug/JicCrl) mice, in which human PBMCs overexpressed *PDCD1^28* (Fig. 7A). Compared to control group, *PDCD1^28*-OE group had a dampened ability to constrain tumor progression, indicated by increased tumor volume (Fig. 7B, C). Consistent with the data from *PDCD1^28^{CKI}* mice, we didn't observe notable change in the frequencies of CD4$^+$ T cells and CD8$^+$ T cells in the spleen of huPBMC-NOG mice compared to control group (Fig. 7D, E). In addition, T_{reg} cells remain largely normal, and no obvious change of Ki-67 expression was observed in splenic CD8$^+$ T cells (Fig. 7F, G).

https://doi.org/10.1038/s41467-024-53561-2

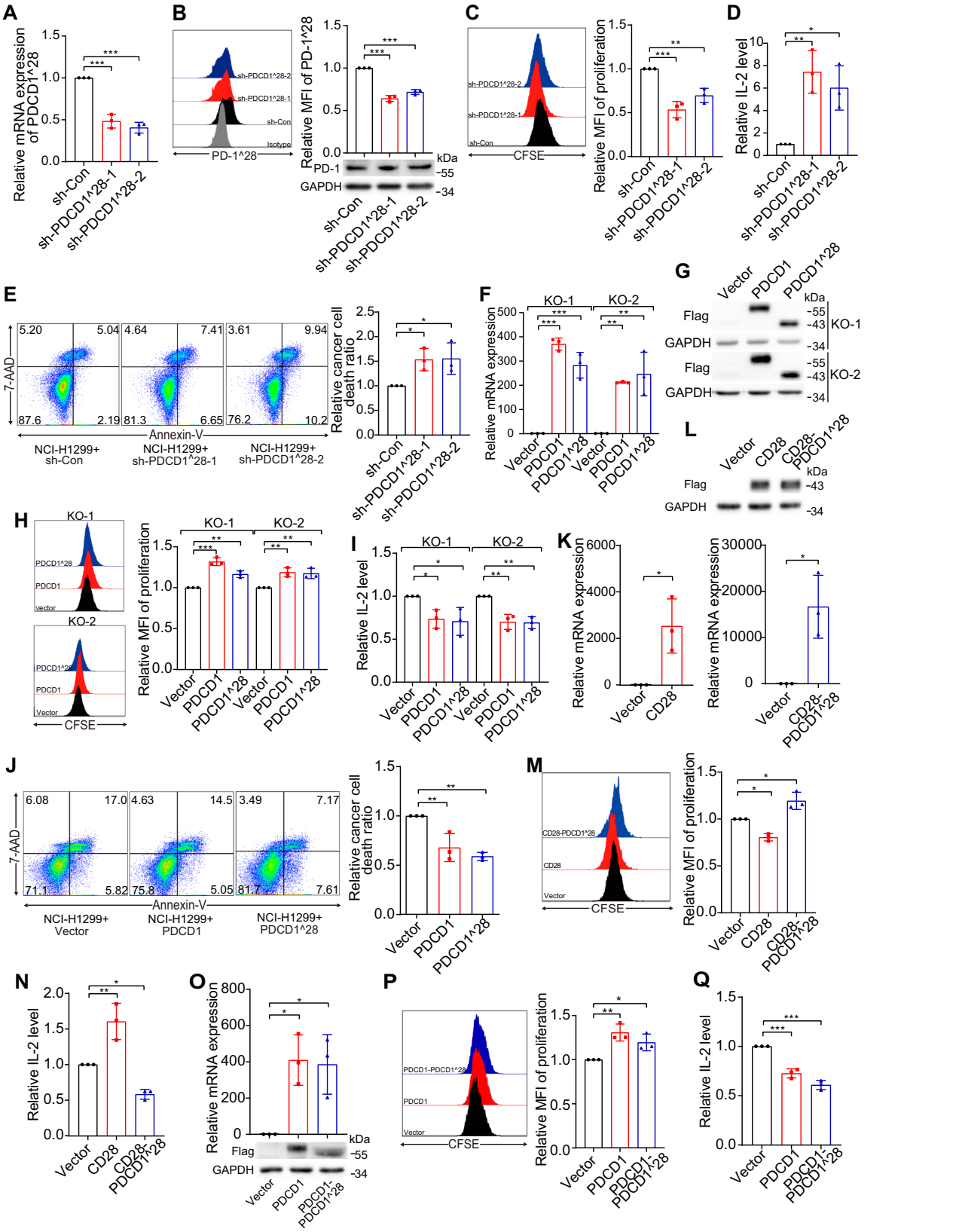

Splenic CD8⁺ T cells displayed lower production of cytokine, including GzmB, IFN-γ, and TNF in the *PDCD1^28*-OE huPBMC-NOG mice (Fig. 7H–J). To understand how PD-1^28 alters the immune landscape of TME in huPBMC-NOG mice, we used FACS to profile tumor-infiltrating immune cell populations. Neither the numbers of both CD4⁺ T cells and CD8⁺ T cells (Fig. 7K, L) nor the proportion of T_{reg} cells (Fig. 7M) were significantly changed compared to controls. *PDCD1^28* OE led to reduced production of cytokines in CD8⁺ T cells (Fig. 7O–Q), but the proliferation remained unchanged (Fig. 7N). Together, these results highlight PD-1^28 as a novel immune checkpoint, negatively regulating anti-tumor immunity in vivo.

Fig. 3 | PD-1^28 negatively regulates the immune function of Jurkat cells. **A**, **B** qRT-PCR analysis for *PDCD1^28* (**A**), or representative FACS (**B**, left), quantified as MFI (**B**, top right) of PD-1^28 and representative immunoblot for PD-1 (**B**, bottom right) in Jurkat cells transfected with the indicated shRNAs ($n = 3$ biologically independent experiments). **C** Representative CFSE assay assessing the relative proliferation (left) and quantified as the MFI (right) in *PDCD1^28* KD Jurkat cells ($n = 3$ biologically independent experiments). **D** Enzyme-linked immunosorbent assay (ELISA) assessing the relative IL-2 production in *PDCD1^28* KD Jurkat cells ($n = 3$ biologically independent experiments). **E** Tumor cell killing of *PDCD1^28* KD Jurkat cells against NCI-H1299 cells. The representative images (left) and the quantified ratio (right) of dead cancer cells measured by Annexin-V and 7-AAD staining ($n = 3$ biologically independent experiments). **F** qRT-PCR analysis for *PDCD1* and *PDCD1^28* in KO-1 and KO-2 Jurkat cells transfected with the indicated plasmids ($n = 3$ biologically independent experiments). **G** Immunoblot analysis for PD-1 and PD-1^28 in KO-1 and KO-2 Jurkat cells transfected with the indicated plasmids. **H** Representative CFSE assay assessing the relative proliferation in KO-1 and KO-2 Jurkat cells with OE of either *PDCD1* or *PDCD1^28* (left). Quantification data as MFI (right) ($n = 3$ biologically independent experiments). **I** ELISA assessing the relative IL-2 production of KO-1 and KO-2 Jurkat cells with OE of either *PDCD1* or *PDCD1^28* ($n = 3$ biologically independent experiments). **J** Tumor cell killing of KO-1 Jurkat cells with OE of either *PDCD1* or *PDCD1^28* against NCI-H1299 cells. The representative images (left) and the quantified ratio (right) of dead cancer cells measured by Annexin-V and 7-AAD staining ($n = 3$ biologically independent experiments). **K**, **L**, **O** qRT-PCR analysis for either wild-type *CD28* (**K**, left) or *CD28-PDCD1^28* (**K**, right) and either wild-type *PDCD1* or *PDCD1-PDCD1^28* (**O**, top), and immunoblot analysis for the indicated proteins (**L** and bottom of **O**) in KO-1 cells transfected with the indicated plasmids ($n = 3$ biologically independent experiments). **M**, **P** Representative CFSE assay assessing the relative proliferation of KO-1 Jurkat cells with OE of either wild-type *CD28* or *CD28-PDCD1^28* (**M**, left), and either wild-type *PDCD1* or *PDCD1-PDCD1^28* (**P**, left). Quantification data as MFI (**M**, **P**, right) ($n = 3$ biologically independent experiments). **N**, **Q** ELISA assessing the relative IL-2 production of KO-1 Jurkat cells with OE of either wild-type *CD28* or *CD28-PDCD1^28* (**N**), and either wild-type *PDCD1* or *PDCD1-PDCD1^28* (**Q**) ($n = 3$ biologically independent experiments). Data represent the mean ± SD. Statistical significance was determined by one-way ANOVA with Dunnett post hoc test (**A**–**F**, **H**–**J**, **M**–**Q**) or two-tailed unpaired Student's *t*-test (**K**). $^{*}p < 0.05$, $^{**}p < 0.01$, $^{***}p < 0.001$. Source data, including exact *p*-values, are provided as a Source Data file.

Discussion

AS is a mechanism to amplify the genetic information for the limited coding-genes and associated with cancer hallmarks[12,13]. Previous studies have shown that AS plays an important role in the expression of immune checkpoint molecules, such as CTLA-4[14,29] and PD-L1[30,31], etc. *PDCD1* generates multiple isoforms through AS[16–18], such as PD-1Δex3 and Δ42PD-1. The soluble isoform PD-1Δex3 lacks exon 3 of *PDCD1*, which plays an antagonistic role by interfering with the signal transduction pathway of PD-1[32]. Δ42PD-1, 42 bp deletion from the start of *PDCD1* exon 2, is expressed by TILs and plays an immunosuppressive role by binding to toll-like receptor-4 to promote progression of hepatocellular carcinoma[33]. Overall, the potential physiological or pathological function of other isoforms remain poorly elucidated. The extracellular domain of PD-1 is secreted into the culture supernatant. However, the cytoplasmic tail of PD-1^28 cannot exist independently in neither the whole cell lysate nor the culture supernatant, which may be due to post-translational modifications or instability of the protein. In addition, we systematically explored the function of PD-1^28 using mouse model in vivo, further demonstrating the potential resistance to ICIs-targeted. However, we failed to identify such isoform in mouse, but this does not rule out the existence with similar function of other isoforms. It is still expectation to explore whether PD-1^28 plays a function in adaptive immune cells or development of immune system and has significance of resistance to ICIs in clinic data. Moreover, we also elucidated that TAF15 mediates the generation of *PDCD1^28* in this study, it is imperative to explore the underlying mechanism of the generation of other isoforms and their physiological or pathological function, which will pave a way for the treatments targeting PD-1/PD-L1 axis.

In conclusion, our study characterizes PD-1^28 transcription and protein expression in T lymphocytes from both healthy human PBMCs and clinical tumor biopsies. PD-1^28 negatively regulates the function of T cells, including proliferation, cytokine production, and tumor cell killing. PD-1^28 confers a previously unrecognized mechanism of resistance to IC therapy (Supplementary Fig. 8).

Methods

Reagents and mice

For human and mouse T cell activation, anti-mouse CD3ε (clone 145-2C11) and anti-mouse CD28 (clone 37.51) were purchased from Biolegend, anti-human CD3 (clone UCHT-1) and anti-human CD28 (clone CD28.2) were purchased from BD Biosciences. Phorbol 12- myristate 13-acetate (PMA, P1585) and PHA (L1668) were purchased from Sigma-Aldrich. Ionomycin (M3621) was purchased from AbMole BioScience.

PDCD1^28$^{flox/flox}$ mice were generated by Cyagen Biosciences (Suzhou, China) on its CRISPR-Cas9 gene targeting platform. The knock-in mice were created at the locus of ROSA26 which is located on mouse chromosome 6 in C57BL/6J mice (#C001089). The CAG promoter-loxP-stop unit-loxP-*PDCD1^28*-rBG pA cassette was inserted between exon 1 and 2 of ROSA26. Homology arms generated by PCR using BAC clone as template. Cas9 and gRNA co-injected into fertilized eggs with targeting vector for mice production. Correctly targeted mice were determined by PCR and gene sequencing. *PDCD1^28$^{flox/flox}$* mice were then crossed with *CD4^{cre}* transgenic mice to obtain *PDCD1^28^{CKI}* mice with PD-1^28 knockin in T cells. For animal experiments with *PDCD1^28^{CKI}* mice, littermate controls with normal PD-1^28 expression (*PDCD1^28$^{flox/flox}$*) were used. *CD4^{cre}* transgenic mice were obtained from Cyagen Biosciences (Suzhou, China, #C001381). NOD.Cg-PrkdcscidIL 2rgtm1Sug/JicCrl (NOG) mice (#408) were purchased from Beijing VitalRiver Laboratory Animal Technology Co. Ltd.

All animal experiments were previously approved by the Ethics Committee for the Use of Experimental Animals of the Suzhou Institute of Biomedical Engineering and Technology, Chinese Academy of Sciences (Suzhou, Jiangsu, China). Monitoring Institute approved all animal protocols used in this study. All mice were maintained under specific pathogen–free conditions. Animals were randomly allocated to experimental groups. All animal experiments used mice with matched age and sex. The animal experiments were performed in a blinded manner.

Cell lines and clinical specimens

The human embryonic kidney HEK293T (GNHu 43) and NCI-H1299 (SCSP-589) cells lines were obtained from the Shanghai Cell Bank Type Culture Collection Committee (Shanghai, China). Jurkat cells (TIB-152) were obtained from the American Type Culture Collection. MC38 (337716) and B16F10 (100309) cells were obtained from BNCC (BeNa Culture Collection). The NCI-H1299, MC38, B16F10 and Jurkat cells were cultured in RPMI1640 medium (Gibco, C11875500BT) supplemented with 10% fetal bovine serum (FBS) (Gibco, 10270). The HEK293T cells were cultured in Dulbecco's modified Eagle medium (DMEM) (Gibco, C11995500BT) supplemented with 10% FBS. All cell lines were verified using short tandem repeat assays (Genetic Testing Biotechnology) and tested negative for mycoplasma contamination. All cells were cultured at 37 °C in an atmosphere of 5% CO_2. Human PBMCs were donated by healthy laboratory members. PBMCs were isolated by gradient centrifugation and enrichment of primary T cells with CD3. Lung cancer samples of patients were obtained from Jiangsu Cancer Hospital. Tumors were freshly isolated and digested. TILs were enriched by density-gradient centrifugation. For intracellular staining of PD-1^28, samples were stained for surface antigens, including CD3, CD4, and CD8, then cells were fixed and permeabilized (BD

https://doi.org/10.1038/s41467-024-53561-2

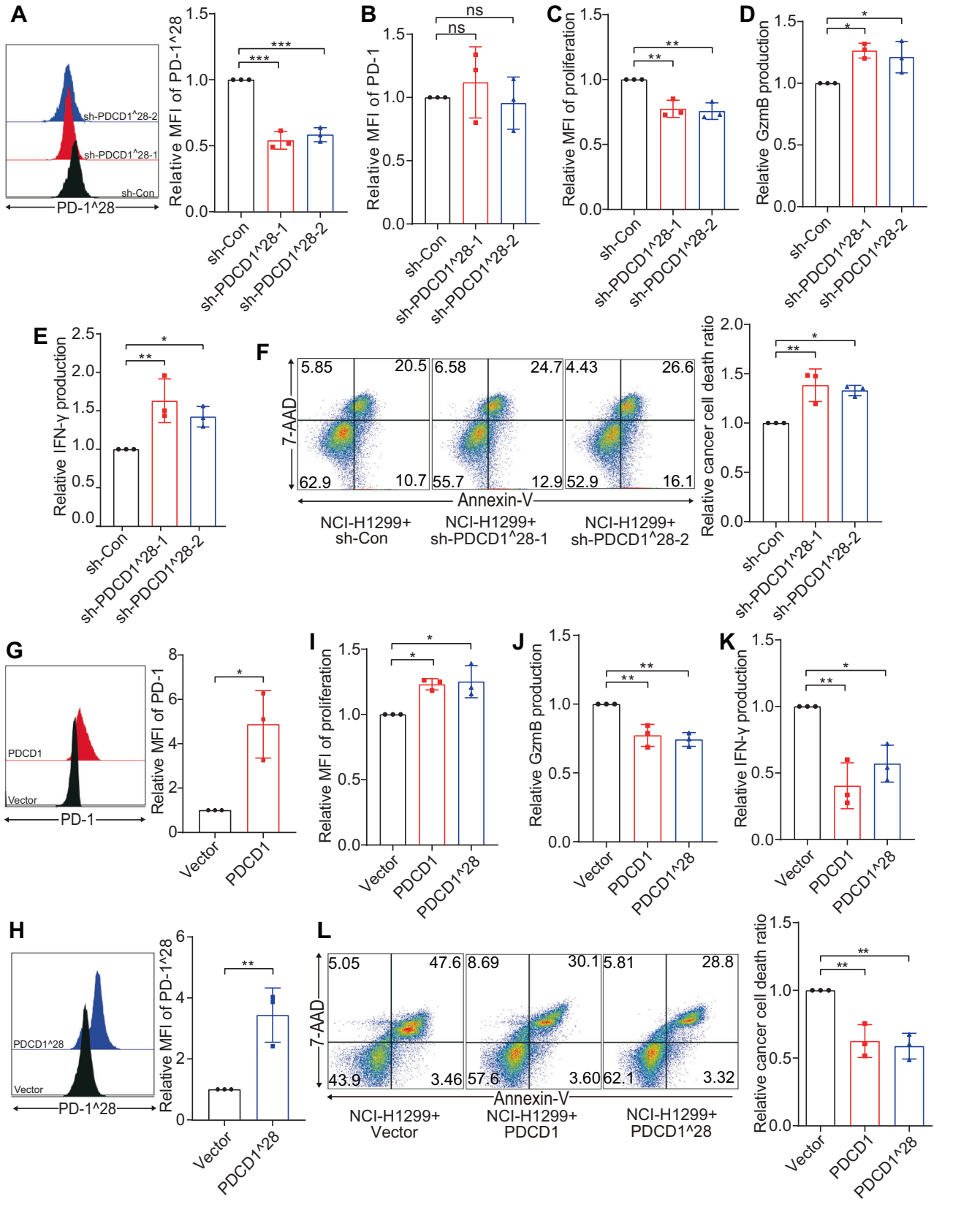

Biosciences, 554714). All of the patients were enrolled with written informed consent. The study was conducted in accordance with the principles of the Declaration of Helsinki and approved by the Institutional Ethical Review Board of Jiangsu Cancer Hospital and complied with all relevant ethical regulations.

RT-PCR and qRT-PCR

Total RNA was isolated from cultured cells using RNAiso Plus (TAKARA, T9109), and complementary DNA (cDNA) was synthesized using PrimeScript RT Master Mix (TAKARA, RR047A) according to the manufacturer's instructions. RT-PCR products were electrophoresed

Fig. 4 | PD-1^28 negatively regulates the immune function of primary T cells. **A** Representative FACS (left) and quantified as MFI (right) for KD efficiency of PD-1^28 in primary T cells isolated from PBMCs transfected with the indicated shRNAs ($n = 3$ biologically independent experiments). **B** FACS assessing PD-1 surface levels and quantified as the MFI in *PDCD1^28* KD primary T cells ($n = 3$ biologically independent experiments). **C** CFSE assay assessing the relative proliferation and quantified as the MFI in *PDCD1^28* KD primary T cells ($n = 3$ biologically independent experiments). **D**, **E** FACS assessing the relative GzmB (**D**) and IFN-γ (**E**) production of *PDCD1^28* KD primary T cells ($n = 3$ biologically independent experiments). **F** Tumor cell killing of *PDCD1^28* KD primary T cells against NCI-H1299 cells. The representative images (left) and the quantified ratio (right) of dead cancer cells measured by Annexin-V and 7-AAD staining ($n = 3$ biologically independent experiments). **G**, **H** Representative FACS (left) and quantified as MFI (right) showing changes in the PD-1 (**G**) or PD-1^28 (**H**) levels of primary T cells transfection with the indicated plasmids ($n = 3$ biologically independent experiments). **I** CFSE assay assessing the relative proliferation and quantified as the MFI of primary T cells with OE of *PDCD1* or *PDCD1^28* ($n = 3$ biologically independent experiments). **J**, **K** FACS assessing the relative GzmB (**J**) and IFN-γ (**K**) production of primary T cells with OE of *PDCD1* or *PDCD1^28* ($n = 3$ biologically independent experiments). **L** Tumor cell killing of primary T cells with OE of *PDCD1* or *PDCD1^28* against NCI-H1299 cells. The representative images (left) and the quantified ratio (right) of dead cancer cells measured by Annexin-V and 7-AAD staining ($n = 3$ biologically independent experiments). Data represent the mean ± SD. Statistical significance was determined by one-way ANOVA with Dunnett post hoc test (**A**–**F**, **I**–**L**) or two-tailed unpaired Student's *t*-test (**G**, **H**). $^{*}p < 0.05$, $^{**}p < 0.01$, $^{***}p < 0.001$. Source data, including exact *p*-values, are provided as a Source Data file.

in 2% agarose gel. qRT-PCR was performed using SYBR premix EX Taq (TaKaRa, RR420A) and analysed with QuantStudio 7 Flex Real-Time PCR System (Thermo Fisher). Relative gene expression was determined by $2^{-\Delta\Delta CT}$ normalized to the housekeeping gene (GAPDH)[34]. The annealing temperature for amplifying endogenous *PDCD1^28* is 68 °C, for amplifying *minigene* is 64 °C, while the rest are amplified at 60 °C. The primers used were listed in Table S5. Transcriptional copy number was measured by using standard curve method and the exact copy number was calculated by relating the CT value to standard curve[35,36]. To measure the value of percent splice in (PSI), we calculate using: $\mathrm{PSI} = \frac{\text{splice in}}{\text{splice in} + \text{splice out}}$.

5′- and 3′-rapid amplification of cDNA ends (RACE)

The 5′-and 3′-RACE analyses were performed to determine the transcriptional initiation and termination sites of *PDCD1^28* based on the nested PCR with three rounds. The primers of three rounds PCR were respectively as following:

5′-RACE: 5′-tccagctccccatagtccacag-3′, 5′-cgacaccaaccaccaggg-3′, and 5′-cttctctccctgccccgggg-3′.

3′-RACE: 5′-aactggtaccgcatgagccc-3′, 5′-cttccacatgagcgtggtca-3′, and 5′- ccccggggcagggagagaag-3′.

RNA-sequencing and analysis

RNA-sequencing of *PDCD1^28* OE and control cells were performed by Berry Genomics (Beijing, China). Raw read counts were used for differential gene expression analysis by DESeq2[37]. Genes with p value < 0.05 and $\log_2$ Fold change (FC) > 1 were counted as upregulated genes, and genes with p value < 0.05 and $\log_2$ FC < −1 were counted as downregulated genes.

Immunoblot (IB)

Whole cell lysates were prepared using Radio Immunoprecipitation Assay (RIPA) lysis buffer (Beyotime Biotechnology, P0013B) containing 1% protease and phosphatase inhibitor cocktails (sigma). Protein concentrations were determined using a BCA protein assay kit (Beyotime Biotechnology, P0012) according to the manufacturer's protocol. Equal amounts of total protein were separated by 10% sodium dodecyl sulfate-polyacrylamide gel electrophoresis (SDS–PAGE) and then transferred onto PVDF membranes (Millipore, ISEQ00010). The membrane was blocked for 1 h in Tris-buffered saline–Tween 20 (TBST) containing 5% nonfat dry milk followed by overnight incubation at 4 °C with the indicated antibodies. After extensive washing, the membrane was incubated with secondary antibody for 1.5 h in blocking buffer. Membranes were washed again, and bands were visualized with the immobilon western horseradish peroxidase substrate kit (Millipore, WBKLS0500). For immunoblots, the detailed information about the antibodies can be found in Table S6. HRP-conjugated goat anti-rabbit and HRP-conjugated goat anti-mouse from Beyotime Technology. Monoclonal antibodies and polyclonal antibodies against PD-1^28 were generated by Genscript. The antigen sequence used were listed in Table S7.

RIP

After stimulation of Jurkat cells with PMA and Ionomycin for 5 h, 5×10^5 cells were washed twice with 10 ml ice-cold phosphate-buffered saline (PBS). Cells were lysed in 150 μl RIP lysis buffer with 1 μl of protease inhibitor cocktail (Sigma, P8340) and 0.5 μl of RNase inhibitor (Beyotime Biotechnology, R0102), and supernatants were collected after centrifugation. 15 μl of supernatant of the RIP lysate was saved as input. Cell lysates were incubated with 15 μl A/G magnetic beads (Millipore, LSKMAGAG10) coated with 1.5 μg anti-TAF15 (proteintech, 24235-1-AP) or IgG (proteintech, 30000-0-AP) antibodies at 4 °C for 5 h. After washing using RIP wash buffer six times, immunoprecipitation or input sample was resuspended in 150 μl of proteinase K buffer (117 μl of RIP Wash Buffer, 15 μl of 10% SDS, and 18 μl of proteinase K) and incubated at 55 °C for 30 min with shaking to digest the protein. Samples were centrifuged, and the supernatants were used to extract RNA by RNeasy Mini Kit (QIAGEN, 74106). Purified RNAs were subjected to cDNA synthesis and then qRT-PCR analysis. In *minigene* overexpressed HEK293T cells, 1.5×10^6 cells were lysed in RIP lysis buffer. Cell lysates were incubated with 15 μl A/G magnetic beads coated with 3 μg anti-TAF15 or IgG at 4 °C for 5 h. The following procedure is the same as described above. The primers used were listed in Table S5.

Immunofluorescence

Immunofluorescence was performed based on a universal protocol. Jurkat cells stimulated with 5 μg/ml PHA for 72 h and untreated Jurkat cells were fixed with 4% paraformaldehyde for 10 min at room temperature and permeabilized with 0.5% Triton X-100 (Sigma, 93443) in PBS. Samples were blocked in 1% donkey serum in the presence of PBS for 1 h and stained with the appropriate primary and secondary antibodies coupled with Alexa Fluor 488 or 647. Confocal images were captured on a confocal microscope (Leica) with a 63× oil objective. The maker of cell membranes were stained with Na/K ATPase. The nuclei were stained with 4′,6-diamidino-2-phenylindole (DAPI).

Immunoprecipitation

Cell lysates were prepared by incubating the cells in IP buffer (50 mM tris-HCl (pH 7.6), 150 mM NaCl, 0.5% Nonidet P-40) in the presence of 1% protease and phosphatase inhibitor cocktails for 20 min at 4 °C. This was followed by centrifugation at 13,400×*g* for 15 min at 4 °C. For immunoprecipitation, protein was incubated with control or PD-1^28 polyclonal antibody for 12 h at 4 °C with constant rotation. Protein A/G magnetic beads was then added and the incubation was continued for an additional 2 h. Beads were then washed six times using the lysis buffer. The precipitated proteins were boiled in 2×loading buffer and subjected to SDS–PAGE followed by immunoblot.

Expression vectors and shRNAs

To generate lentiviruses expressing the indicated shRNAs or indicated genes, HEK293T cells were transfected with shRNAs (cloned in pSIH-

https://doi.org/10.1038/s41467-024-53561-2

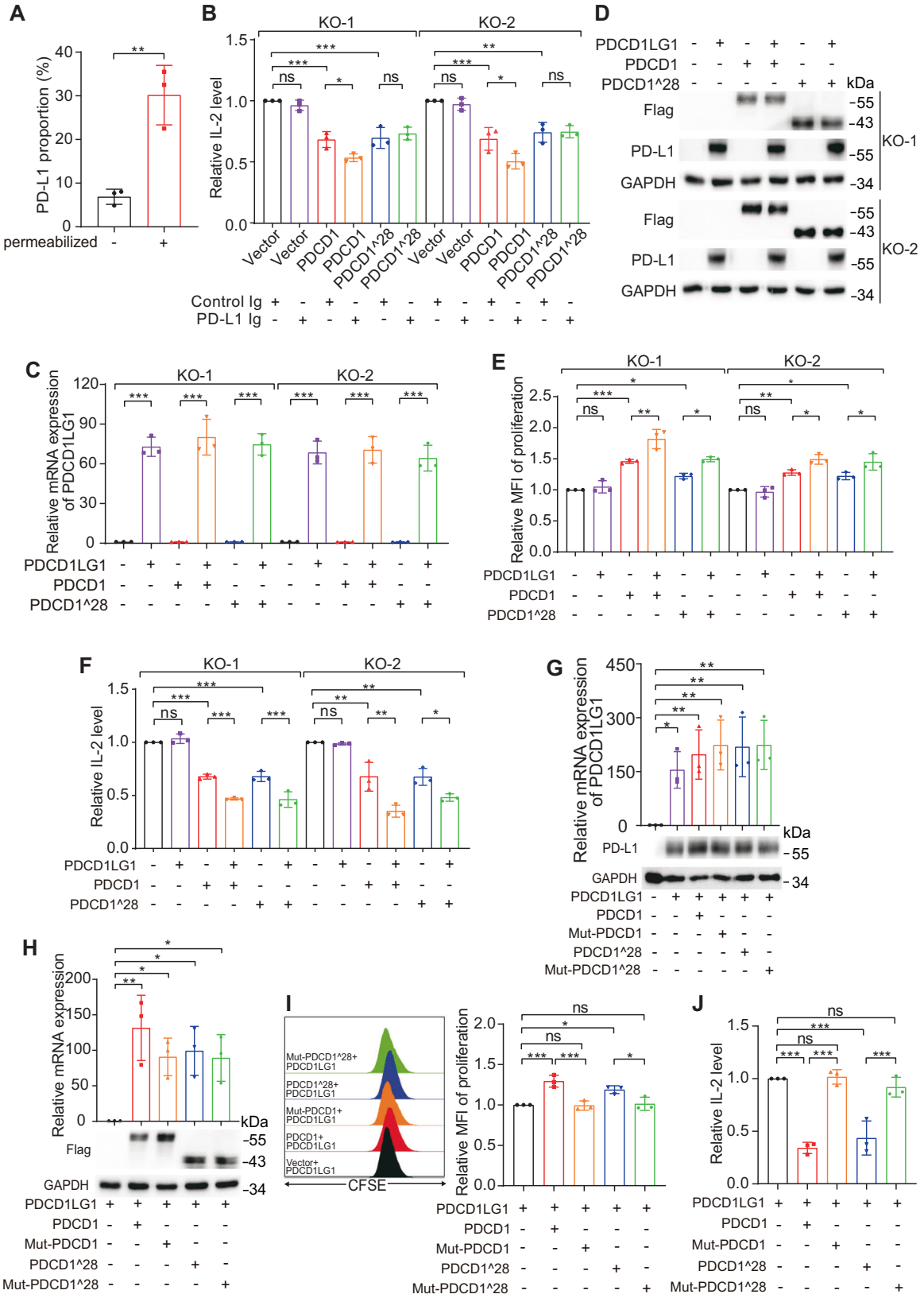

H1-Puro) or full-length genes with 3×FLAG on the C′-terminus (cloned into pLVX-IRES-Neo), PMD2.G and psPAX2 with a ratio of 8: 3: 6. For generation of the control virus, pSIH-H1-Puro or pLVX-IRES-Neo empty vector was used. The supernatant was collected 48 h after transfection and centrifuged at 1,400 x g for 10 min, and the supernatant was used for infection. The efficiencies of lentivirus-mediated KD and OE were verified by qRT-PCR or immunoblot analysis respectively. The shRNA sequences were shown in Table S8. The KO efficiency of *PDCD1* in Jurkat cells was confirmed by genomic DNA sequencing and immunoblot analysis.

https://doi.org/10.1038/s41467-024-53561-2

Fig. 5 | PD-1^28 binding with PD-L1 inhibits T cells activation. A FACS analysis for PD-L1 proportion in Jurkat cells with intact or permeabilized membrane ($n = 3$ biologically independent experiments). **B** ELISA assessing the relative IL-2 production of KO-1 and KO-2 Jurkat cells transfected with the indicated plasmids and treated with either Ig or PD-L1 Ig ($n = 3$ biologically independent experiments). **C**, **D** qRT-PCR analysis for *PDCD1LG1* (**C**) and immunoblot analysis of the indicated proteins (**D**) in KO-1 and KO-2 Jurkat cells transfected with the indicated plasmids ($n = 3$ biologically independent experiments). **E**, **F** CFSE assay assessing the relative proliferation and quantified as MFI (**E**), or ELISA assessing the relative IL-2 production (**F**) of KO-1 and KO-2 Jurkat cells transfected with the indicated plasmids ($n = 3$ biologically independent experiments). **G** qRT-PCR analysis for *PDCD1LG1* (top) and immunoblot (bottom) in KO-1 Jurkat cells transfected with the indicated plasmids ($n = 3$ biologically independent experiments). **H** qRT-PCR analysis for wild-type *PDCD1*, mutant *PDCD1*, wild-type *PDCD1^28* and mutant *PDCD1^28* (top) and immunoblot (bottom) in KO-1 Jurkat cells transfected with the indicated plasmids ($n = 3$ biologically independent experiments). **I**, **J** Representative CFSE assay assessing the relative proliferation (**I**, left) and quantification data as MFI (**I**, right), or ELISA assessing the relative IL-2 production (**J**) of KO-1 Jurkat cells transfected with the indicated plasmids ($n = 3$ biologically independent experiments). Data represent the mean ± SD. Statistical significance was determined by two-tailed unpaired Student's *t*-test (**A**) or one-way ANOVA with Tukey (**B**, **C**, **E**, **F**, **I**, **J**) or Dunnett (**G**, **H**) post hoc test. $^{*}p < 0.05$, $^{**}p < 0.01$, $^{***}p < 0.001$. Source data, including exact *p*-values, are provided as a Source Data file.

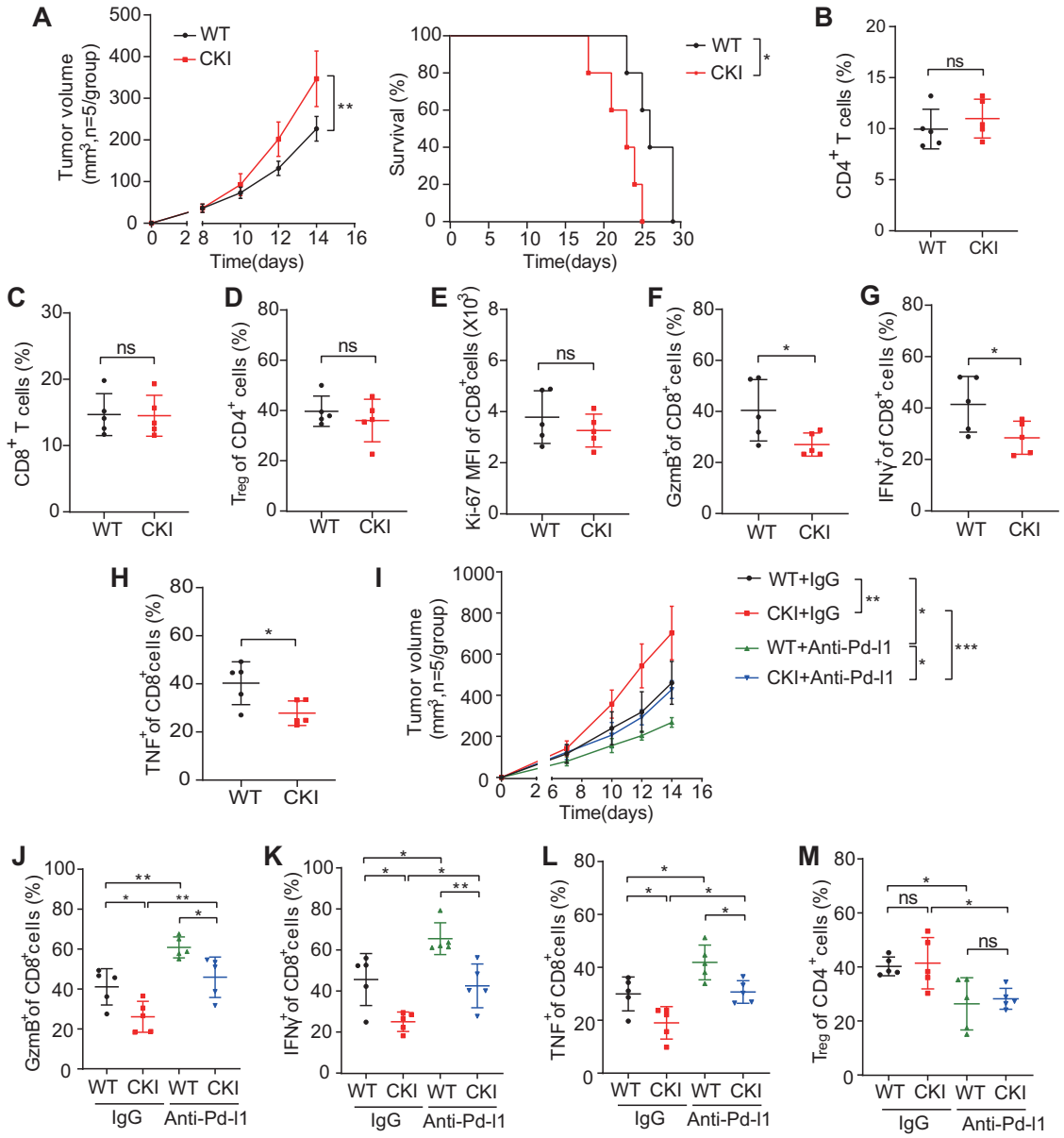

Fig. 6 | PD-1^28 regulates T cell anti-tumor immunity in MC38 colorectal carcinoma mouse model. A Tumor progression of MC38 colorectal carcinoma, indicated by tumor volume in mice (left) and the survival of mice (right) assessed in control and *PDCD1^28^CKI* mice ($n = 5$). **B**–**H** Tumor-infiltrating T cells isolated and analyzed after transplantation ($n = 5$). Frequencies of $CD4^+$ T cells (**B**), $CD8^+$ T cells (**C**), and T_{reg} cell population (**D**). Quantified results of Ki-67 (**E**), GzmB (**F**), IFN-γ (**G**), and TNF (**H**) expressions of $CD8^+$ TILs in the tumor microenvironment. **I**–**M** Anti-Pd-l1 therapy against MC38 colorectal carcinoma ($n = 5$). Tumor volume (**I**), GzmB (**J**), IFN-γ (**K**), and TNF (**L**) expressions of $CD8^+$ TILs and population of T_{reg} cells (**M**) measured. Data represent the mean ± SD. Statistical significance was determined by two-tailed unpaired Student's *t*-test (**A**, left and **B**–**H**), log-rank (Mantel-Cox) test (**A**, right), or one-way ANOVA with Tukey post hoc test (**I**–**M**). $^{*}p < 0.05$, $^{**}p < 0.01$, $^{***}p < 0.001$. Source data, including exact *p*-values, are provided as a Source Data file.

https://doi.org/10.1038/s41467-024-53561-2

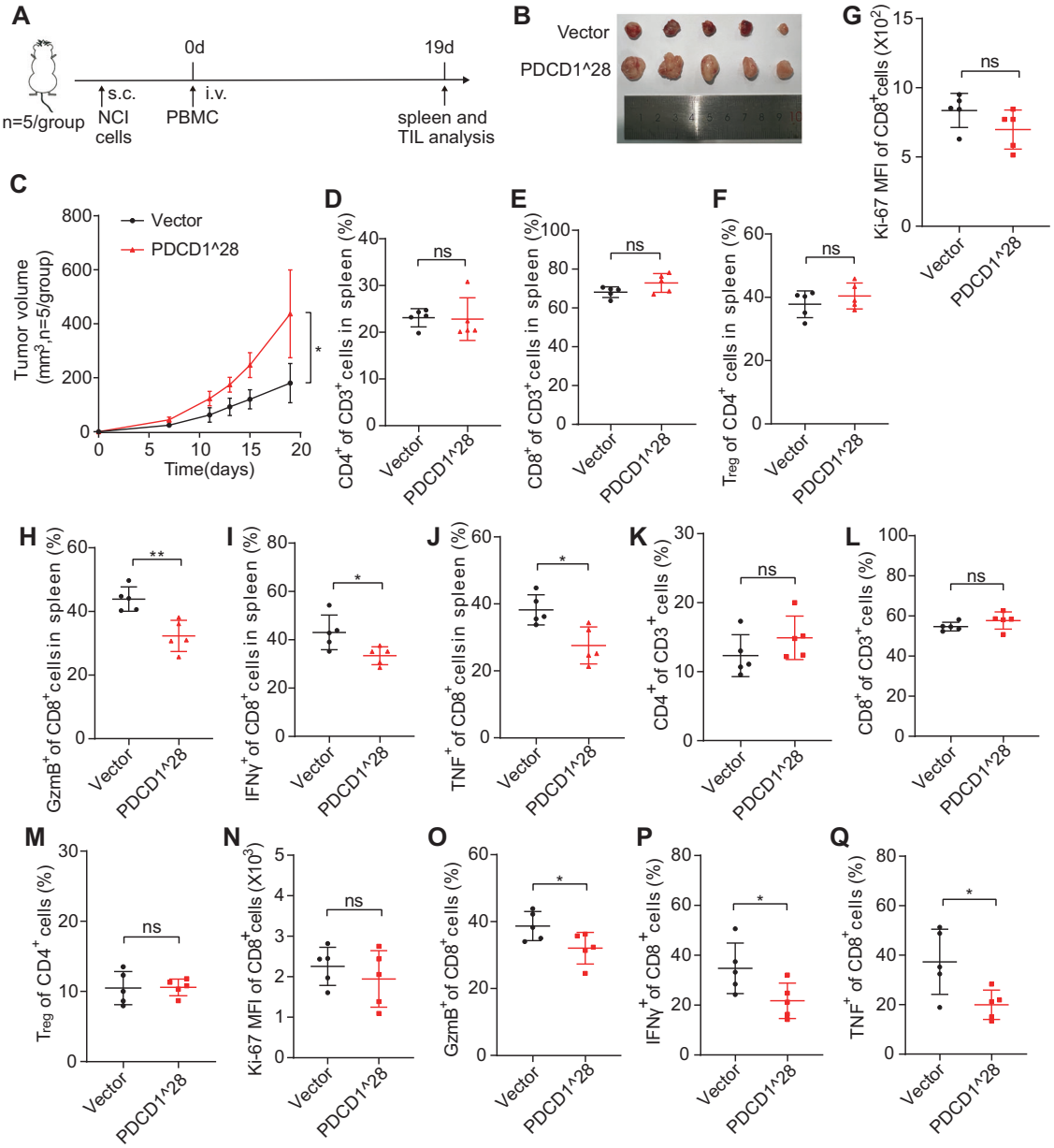

Fig. 7 | PD-1^28 regulates T cell anti-tumor immunity in huPBMC-NOG mouse model. A Experimental design of huPBMC-NOG mice model. PBMCs respectively transfected with a control and *PDCD1^28*. s.c., subcutaneous; i.v., intravenous. **B** Tumor size in control and *PDCD1^28* OE huPBMC-NOG mice subcutaneously implanted with NCI-H1299 cells at the end point ($n = 5$). **C** Effects of PD-1^28 on tumor growth in subcutaneously implanted huPBMC-NOG mice ($n = 5$). **D**–**J** Phenotypic assessment of T cells in spleens isolated from control ($n = 5$) or *PDCD1^28* OE huPBMC-NOG mice ($n = 5$). Frequency of $CD4^+$ T cells (**D**), $CD8^+$ T cells (**E**), and T_{reg} cell population (**F**). Quantified results of Ki-67 (**G**), GzmB (**H**), IFN-γ (**I**), and TNF (**J**) expressions of $CD8^+$ T cells in the spleen. **K**–**Q** TILs of control ($n = 5$) and *PDCD1^28* OE huPBMC-NOG mice ($n = 5$) isolated and analyzed after transplantation. Frequencies of $CD4^+$ T cells (**K**), $CD8^+$ T cells (**L**), and T_{reg} cell population (**M**). Quantified results of Ki-67 (**N**), GzmB (**O**), IFN-γ (**P**), and TNF (**Q**) expressions of $CD8^+$ TILs in the tumor microenvironment. Data represent the mean ± SD. Statistical significance was determined by two-tailed unpaired Student's t-test (**C**–**Q**). $^*p < 0.05$, $^{**}p < 0.01$, $^{***}p < 0.001$. Source data, including exact *p*-values, are provided as a Source Data file.

Cell proliferation assay

To assess the proliferation of lymphocytes and Jurkat cells, Carboxyfluorescein Succinimidyl Ester (CFSE), a dye for the tracking of cell division (Thermo Fisher, C34554) was used. A total of 1×10^6 T cells or Jurkat cells were stained with CFSE (5 μM). The cells were then incubated at 37 °C for 20 min and the reaction was stopped by adding 5 volumes of medium with 10% FBS. 1×10^6 CFSE-labeled cells were seeded into a 6 cm dish and add 3 μg/ml PHA at the same time. After incubation for 48 h, cells were harvested, and the proliferation of T cells was determined and analyzed by CFSE dilution. The intensity of CFSE staining were scored according to the MFI of FITC measured and analysed by FACS.

ELISA

Levels of IL-2 production were measured by enzyme-linked immunosorbent assay (ELISA) in Jurkat cell culture supernatants. After cells were stimulated with PMA and ionomycin for 4-6 h, cells were inoculated into a 96 well plate with 3.5×10^4 cells per well, and the supernatant was collected 48 h later. *PDCD1^28* KD Jurkat cells stimulated by 5 μg/ml plate-coated anti-CD3 antibody and collected 24 h later. The secretion of IL-2 in the supernatants was analyzed using the human IL-2 ELISA Kit (Thermo Fisher, 88-7025-76), following the manufacturer's protocol.

T cell-mediated tumor cell killing assay

To assess the cytotoxic function of lymphocytes and Jurkat cells against tumor cells, the isolated lymphocytes or Jurkat cells were stimulated with PMA and ionomycin for 4-6 h. The stimulated lymphocytes or Jurkat cells (10×10^4 cells) were co-cultured with CFSE-labeled NCI-H1299 cells (5×10^4 cells) in 6-well plates, maintaining an effector to target (E:T) ratio of 2:1. After 60 h of co-culture, both floating and adherent cells were collected, Annexin V staining in combination with 7-AAD (Biolegend, 640930) was used to measure killing efficiency and by FACS. Briefly, cells were then harvested and transferred to Falcon polystyrene tubes, washed with cold PBS for twice and resuspended with 100 μl 1×Annexin V binding buffer. 5 μl Annexin V/7-AAD solution was added to each tube and a further 400 μl of 1×Annexin V binding buffer added after 15 min incubation in the dark. Samples were subjected to FACS analysis within 1 h.

Mouse peripheral T cell isolation and effector function analysis

Peripheral naive $CD8^+$ cells were isolated from the *PDCD1^28*$^{flox/flox}$ and *PDCD1^28*^{CKI} mice ($n = 5$ mice per group, female, age of 6–8 weeks) spleen by negative selection magnetic beads (STEM CELL Technologies, 19853). Naive $CD8^+$ T cells were stimulated with plate-bound anti-CD3/CD28 in the presence of IL-2 for 72 h. To examine cytokine secretion, 5 μg/ml Brefeldin A (BFA) (Biolegend, 420601) was added 5 h before cells were collected to block cytokine transportation. The following procedure for cytokine detection by FACS as the described mouse models below. To measure the proliferation of T cells, naive $CD8^+$ T cells were stained with 5 μM CFSE. The cells were then incubated at 37 °C for 20 min and the reaction was stopped by adding 5 volumes of medium with 10% FBS. CFSE-labeled cells were collected for FACS analysis after activation by plate-bound anti-CD3/CD28.

Mouse models

For the MC38 colorectal carcinoma and B16F10 melanoma mouse models, 3×10^6 MC38 cells or 2×10^6 B16F10 cells were suspended in PBS and injected subcutaneously of *PDCD1^28*$^{flox/flox}$ and *PDCD1^28*^{CKI} mice ($n = 5$ mice per group, female, age of 6–8 weeks). For anti-Pd-l1 therapy experiments, anti-PD-L1 (clone 10 F.9G2) and IgG (clone LTF-2) antibodies were purchased from BioXCell. *PDCD1^28*$^{flox/flox}$ and *PDCD1^28*^{CKI} mice ($n = 5$ mice per group, female, age of 6–8 weeks) were intraperitoneally injected with IgG or anti-Pd-l1 antibody (200 μg per mouse, dissolved in PBS) every three days (three times in total) starting 1 day before the volume of the tumors reached 150-200 mm^3. For the PBMC-engrafted humanized NOG mouse model, NOG mice ($n = 5$ mice per group, male, age of 6–8 weeks) were injected subcutaneously with 9×10^6 NCI-H1299 cells. A total of 10×10^6 *PDCD1^28*-OE and control PBMCs were injected into the tail vein 7 days after cancer cell injection. Tumor formation/growth was assessed as a time course until the experimental endpoint. Mice bearing a tumor were monitored every 2–4 days. We used a vernier caliper to record the length and width of the tumor separately and tumor volume was calculated by the formula: $(\text{width})^2 \times \text{length}/2$. Maximal tumor size allowed by the Institutional Animal Care and Use Committee guidelines at Suzhou Institute of Biomedical Engineering and Technology is 2.0 centimeters (cm) in any direction and we have adhered to these size limits in all mice experiments. Tumor ulceration or moribund condition also require euthanasia. Mice were euthanized by cervical dislocation by trained and experienced staff. In order to analyse the phenotype of TILs, tumor tissues were digested using a mechanical method to obtain a single-cell suspension. The tumor tissues were manually dissected into 1–3 mm pieces using a surgical scalpel. The tissues were then chopped into single cells by gently grinding through 70-μm filters and 200-μm nylon mesh, respectively. The Mouse TIL Isolation Kit (Solarbio, P9000) was utilized to remove cancer cells and enrich leukocytes from the tumor tissues. The isolation procedure was carried out according to the instructions provided by the manufacturer. Spleens were surgically removed with sterilized surgical equipment and crushed using the blunt end of a 1 ml syringe on Petri dishes containing 5 ml of PBS. The spleen mixtures were then individually filtered through a 70 μm filter into a 50 ml conical tube, centrifuged at 200×*g* for 5 min at room temperature. After wash, cell pellets were resuspended in 5 ml of red blood cell lysis solution (Beyotime Biotechnology, C3702) on ice for 5 min and stopped by addition of 30 ml of PBS. After wash, cells were then filtered through 200 mesh filter into 15 ml conical tubes.

Live cells were first stained with Fixable Viability Stain 620 staining (BD Biosciences, 564996). Surface staining, such as CD45, CD3, CD4, CD8, CD127, and CD25, was carried out on ice in PBS containing 2% bovine serum albumin (BSA) or FBS for 30 min, and Ki-67 staining was performed with a Foxp3/Transcription Factor Staining Buffer Set (00-5523-00, eBioscience) according to the manufacturer's protocol. To measure the effector function of $CD8^+$ T cells, cells were stimulated with PMA plus ionomycin with BFA according to the manufacturer's instructions (Biolegend, 423303). After 5 h, cells were stained for dead cells and surface markers. Then, the cells were fixed and permeabilized according to the manufacturer's instructions and subsequently stained with cytokine antibodies. Detailed information about the antibodies can be found in Table S6. Data were analyzed using FlowJo (version V10).

Statistical analysis

Data was presented as the mean ± standard error of the mean (SEM) or standard deviation (SD). Statistical differences between two experimental groups were determined using the two-tailed unpaired Student's *t*-test, or in the case of three or more experimental groups, one-way ANOVA with Dunnett or Tukey post hoc test. Survival was measured by the Kaplan-Meier method, and survival curves were analyzed using the log-rank (Mantel-Cox) test. p value < 0.05 was considered statistically significant. All statistical analyses and graph plotting were performed with GraphPad Prism 8.0.2. $^*p < 0.05$, $^{**}p < 0.01$, $^{***}p < 0.001$; ns, not significant.

Reporting summary

Further information on research design is available in the Nature Portfolio Reporting Summary linked to this article.

Data availability

The RNA-seq raw data have been deposited in the Gene Expression Omnibus (GEO) database under the accession code GSE244939. All data are included in the Supplementary Information or available from the authors, as are unique reagents used in this Article. The raw numbers for charts and graphs are available in the Source Data file whenever possible. Source data are provided with this paper.

References

1. Pardoll, D. M. The blockade of immune checkpoints in cancer immunotherapy. *Nat. Rev. Cancer* **12**, 252–264 (2012).
2. Nurieva, R. I., Liu, X. & Dong, C. Yin-Yang of costimulation: crucial controls of immune tolerance and function. *Immunol. Rev.* **229**, 88–100 (2009).
3. Ishida, Y., Agata, Y., Shibahara, K. & Honjo, T. Induced expression of PD-1, a novel member of the immunoglobulin gene superfamily, upon programmed cell death. *EMBO J.* **11**, 3887–3895 (1992).
4. Keir, M. E., Butte, M. J., Freeman, G. J. & Sharpe, A. H. PD-1 and its ligands in tolerance and immunity. *Annu. Rev. Immunol.* **26**, 677–704 (2008).
5. Wang, X. et al. Tumor cell-intrinsic PD-1 receptor is a tumor suppressor and mediates resistance to PD-1 blockade therapy. *Proc. Natl Acad. Sci. USA* **117**, 6640–6650 (2020).

6. Freeman, G. J. et al. Engagement of the PD-1 immunoinhibitory receptor by a novel B7 family member leads to negative regulation of lymphocyte activation. *J. Exp. Med.* **192**, 1027–1034 (2000).
7. Latchman, Y. et al. PD-L2 is a second ligand for PD-1 and inhibits T cell activation. *Nat. Immunol.* **2**, 261–268 (2001).
8. Jenkins, R. W., Barbie, D. A. & Flaherty, K. T. Mechanisms of resistance to immune checkpoint inhibitors. *Br. J. Cancer* **118**, 9–16 (2018).
9. Sharma, P., Hu-Lieskovan, S., Wargo, J. A. & Ribas, A. Primary, adaptive, and acquired resistance to cancer immunotherapy. *Cell* **168**, 707–723 (2017).
10. Blencowe, B. J. Alternative splicing: new insights from global analyses. *Cell* **126**, 37–47 (2006).
11. Wang, Y. et al. Mechanism of alternative splicing and its regulation. *Biomed. Rep.* **3**, 152–158 (2015).
12. Venables, J. P. Aberrant and alternative splicing in cancer. *Cancer Res.* **64**, 7647–7654 (2004).
13. Oltean, S. & Bates, D. O. Hallmarks of alternative splicing in cancer. *Oncogene* **33**, 5311–5318 (2014).
14. Ward, F. J. et al. The soluble isoform of CTLA-4 as a regulator of T-cell responses. *Eur. J. Immunol.* **43**, 1274–1285 (2013).
15. Lynch, K. W. Consequences of regulated pre-mRNA splicing in the immune system. *Nat. Rev. Immunol.* **4**, 931–940 (2004).
16. Nielsen, C., Ohm-Laursen, L., Barington, T., Husby, S. & Lillevang, S. T. Alternative splice variants of the human PD-1 gene. *Cell Immunol.* **235**, 109–116 (2005).
17. Zhou, J. et al. Potentiating functional antigen-specific $CD8^+$ T cell immunity by a novel PD1 isoform-based fusion DNA vaccine. *Mol. Ther.* **21**, 1445–1455 (2013).
18. Ponce de León, C. et al. Significance of PD1 alternative splicing in celiac disease as a novel source for diagnostic and therapeutic target. *Front. Immunol.* **12**, 678400 (2021).
19. Agata, Y. et al. Expression of the PD-1 antigen on the surface of stimulated mouse T and B lymphocytes. *Int. Immunol.* **8**, 765–772 (1996).
20. Esensten, J. H., Helou, Y. A., Chopra, G., Weiss, A. & Bluestone, J. A. CD28 costimulation: from mechanism to therapy. *Immunity* **44**, 973–988 (2016).
21. Iwai, Y. et al. Involvement of PD-L1 on tumor cells in the escape from host immune system and tumor immunotherapy by PD-L1 blockade. *Proc. Natl Acad. Sci. USA* **99**, 12293–12297 (2002).
22. Tu, X. et al. PD-L1 (B7-H1) competes with the RNA exosome to regulate the DNA damage response and can be targeted to sensitize to radiation or chemotherapy. *Mol. Cell* **74**, 1215–1226.e1214 (2019).
23. Ying, H. et al. Non-cytomembrane PD-L1: An atypical target for cancer. *Pharmacol. Res.* **170**, 105741 (2021).
24. Francisco, L. M. et al. PD-L1 regulates the development, maintenance, and function of induced regulatory T cells. *J. Exp. Med.* **206**, 3015–3029 (2009).
25. Lin, D. Y. et al. The PD-1/PD-L1 complex resembles the antigen-binding Fv domains of antibodies and T cell receptors. *Proc. Natl Acad. Sci. USA* **105**, 3011–3016 (2008).
26. Zak, K. M. et al. Structure of the complex of human programmed death 1, PD-1, and its ligand PD-L1. *Structure* **23**, 2341–2348 (2015).
27. Magiera-Mularz, K. et al. Human and mouse PD-L1: similar molecular structure, but different druggability profiles. *iScience* **24**, 101960 (2021).
28. Li, N. et al. Tumor perfusion enhancement by ultrasound stimulated microbubbles potentiates PD-L1 blockade of MC38 colon cancer in mice. *Cancer Lett.* **498**, 121–129 (2021).
29. Liu, S. M. et al. Overexpression of the Ctla-4 isoform lacking exons 2 and 3 causes autoimmunity. *J. Immunol.* **188**, 155–162 (2012).
30. Gong, B. et al. Secreted PD-L1 variants mediate resistance to PD-L1 blockade therapy in non-small cell lung cancer. *J. Exp. Med.* **216**, 982–1000 (2019).
31. Zheng, X., Chen, X. & Wu, W. The regulatory axis of PD-L1 isoform 2/TNF/T cell proliferation is required for the canonical immune-suppressive effects of PD-L1 isoform 1 in liver cancer. *Int. J. Mol. Sci.* **24**, 6314 (2023).
32. Sun, J., Bai, J., Jiang, T., Gao, Y. & Hua, Y. Modulation of PDCD1 exon 3 splicing. *RNA Biol.* **16**, 1794–1805 (2019).
33. Tan, Z. et al. Isoformic PD-1-mediated immunosuppression underlies resistance to PD-1 blockade in hepatocellular carcinoma patients. *Gut* **72**, 1568–1580 (2023).
34. Livak, K. J. & Schmittgen, T. D. Analysis of relative gene expression data using real-time quantitative PCR and the 2(-Delta Delta C(T)) Method. *Methods* **25**, 402–408 (2001).
35. Qu, L. et al. Exosome-transmitted lncARSR promotes sunitinib resistance in renal cancer by acting as a competing endogenous RNA. *Cancer cell* **29**, 653–668 (2016).
36. Gu, Y. et al. DMDRMR-mediated regulation of m(6)A-modified CDK4 by m(6)A reader IGF2BP3 drives ccRCC progression. *Cancer Res.* **81**, 923–934 (2021).
37. Love, M. I., Huber, W. & Anders, S. Moderated estimation of fold change and dispersion for RNA-seq data with DESeq2. *Genome Biol.* **15**, 550 (2014).

Acknowledgements

This work was supported by the National Natural Science Foundation of China 82150114 (to S.G.) and 82203348 (to Y.G.); by grants from the Fundamental Research Funds for the Central Universities (to S.G.); by grants from the National Key Research and Development Program of China 2022YFC3401001 (to S.G.); by grants from the Nanjing Postdoctoral Research Grant (to M.S.); by grants from the China Postdoctoral Science Foundation 2024T170422 (to M.S.).

Author contributions

X.W. and S.G. designed research; R.Y. provided samples; X.W., T.L., Y.L., A.D., Y.G., J.Z., T.C., S.W., and C.Z. performed research; X.W., S.C., L.D., M.S., and S.G. analysed the data; X.W., X.Z., and S.G. wrote the paper.

Competing interests

The authors declare no competing interests.

Additional information

Supplementary information The online version contains supplementary material available at https://doi.org/10.1038/s41467-024-53561-2.

Correspondence and requests for materials should be addressed to Shan Gao.

Peer review information *Nature Communications* thanks the anonymous reviewer(s) for their contribution to the peer review of this work. A peer review file is available.